ACS Catalysis

pubs.acs.org/acscatalysis

Research Article

Role of Bifunctional Ru/Acid Catalysts in the Selective Hydrocracking of Polyethylene and Polypropylene Waste to Liquid Hydrocarbons

Julie E. Rorrer, Amani M. Ebrahim, Ydna Questell-Santiago, Jie Zhu, Clara Troyano-Valls, Arun S. Asundi, Anna E. Brenner, Simon R. Bare, Christopher J. Tassone, Gregg T. Beckham, and Yuriy Román-Leshkov*

Cite This: *ACS Catal.* 2022, 12, 13969−13979

Read Online

ACCESS | Metrics & More | Article Recommendations | Supporting Information

ABSTRACT: Hydrogenolysis of C−C bonds over Ru-based catalysts has emerged as a deconstruction strategy to convert single-use polyolefin waste to liquid alkanes at relatively mild conditions, but this approach exhibits limitations, including methane formation resulting from terminal C−C bond scission. In this study, a variety of catalysts were investigated for the reductive deconstruction of polyethylene (PE) and polypropylene (PP) to identify supports that promote nonterminal C−C bond scission. We found that Ru nanoparticles supported on Brønsted-acidic zeolites with the faujasite (FAU) and Beta (BEA) topologies were highly active for the cleavage of C−C bonds in PE and PP, exhibiting improved liquid yields and suppressed methane formation. For the deconstruction of PE, supporting ruthenium nanoparticles (5 wt %) on FAU increased the yields of liquid alkanes to 67% compared to 33% over an inert silica support (5 wt % Ru/SiO_2) at 200 °C, 16 h, under 30 bar of H_2. A dramatic selectivity enhancement toward liquid hydrocarbons was also observed for PP over Ru/FAU and Ru/BEA compared to Ru/SiO_2. To understand the origin of this selectivity improvement, a combination of *ex situ* and *operando* characterization techniques were used to reveal that both catalyst structure and acidity play key roles in PE and PP conversion. *Operando* X-ray absorption spectroscopy studies with model polyolefins over Ru-supported catalysts with varying acidity levels revealed that the local chemical environment of $Ru^{[0]}$ during the reaction is consistent across multiple acidic supports, although the onset of reduction during synthesis of the nanoparticles varies across different supports. These results, combined with reactivity data, demonstrate the importance of the acid-noble metal cooperativity in promoting selective C−C bond scission toward liquid alkanes that shifts the mechanism from hydrogenolysis to ideal hydrocracking.

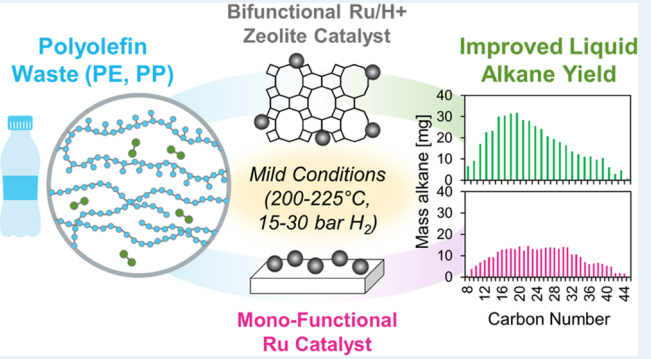

KEYWORDS: *plastic upcycling, hydrogenolysis, hydrocracking, polypropylene, polyethylene, depolymerization, ruthenium, bifunctional catalyst*

INTRODUCTION

The versatility and low production cost of plastic materials has resulted in massive global consumption of single-use plastic for food packaging, medical devices, consumer goods, and numerous other products. Approximately 380 million tons of plastics are generated each year,[1] and it is projected that production will reach over 1.1 billion tons per year by 2050.[2] Polyethylene (PE) and polypropylene (PP) are among the most widely produced plastics, accounting for approximately 42% of all plastic consumed.[3] Unfortunately, traditional recycling methods are unable to keep up with the rapid generation of plastic waste, resulting in enormous quantities of end-of-life plastics entering landfills and leaking into the environment. Globally, only around 16% of plastic waste is recycled.[4] In the United States, recycling rates for poly(ethylene terephthalate) (PET), high-density PE (HDPE), PP, and low-density/linear-low-density PE (LDPE/LLDPE) in 2019 were 15, 10, 3, and 2% respectively, and landfill rates were 76, 82, 88, and 88%, respectively.[5] These high landfill rates contribute to significant economic losses, with an estimated market value of $7.2 billion (2019).[5] Chemical upcycling, defined as an open-loop chemical recycling process where the remanufactured products exhibit a higher value than

Received: July 23, 2022
Revised: October 13, 2022

https://doi.org/10.1021/acscatal.2c03596
ACS Catal. 2022, 12, 13969−13979

Scheme 1. Proposed Scheme for Ideal Hydrocracking of PE (Top) and PP (Bottom) over Ruthenium Nanoparticles Supported on Brønsted-Acidic Supports

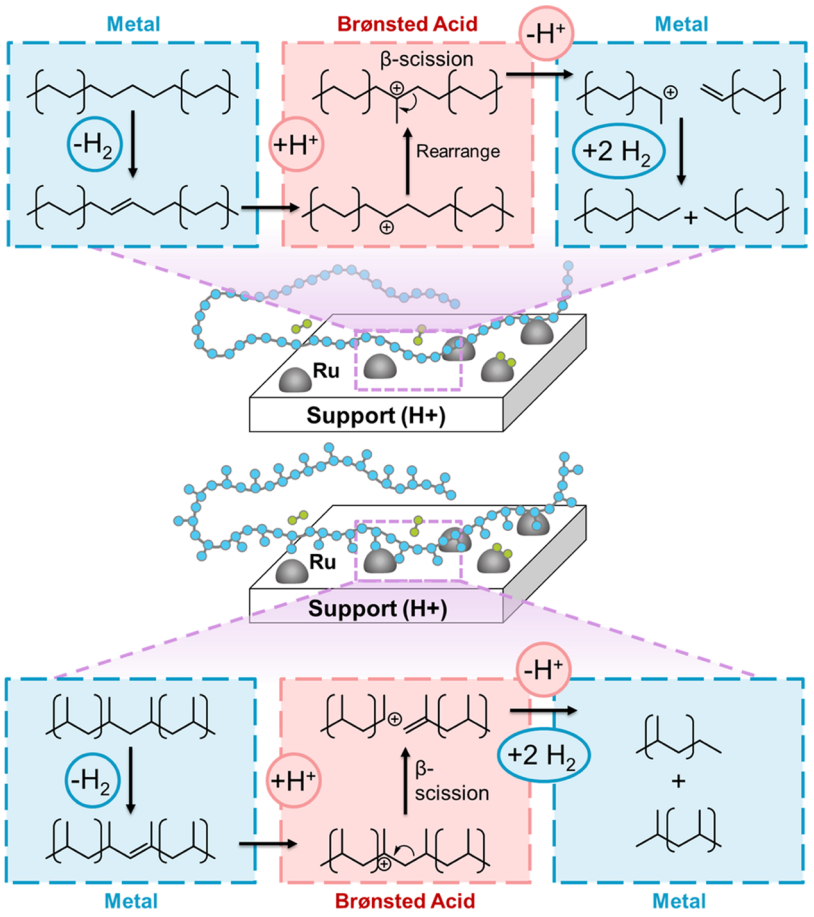

the original plastic waste, is one strategy to divert this waste from landfills and the environment.[6]

Despite being the most widely produced plastics, polyolefins have traditionally received less attention for chemical recycling in the academic literature than PET, largely due to the difficulty of cleaving strong C−C bonds in the backbone.[7] The most common chemical recycling strategies for polyolefins are gasification and pyrolysis, but both methods suffer from low product selectivity and require high temperatures and harsh operating conditions.[8−10] Several recent reviews have highlighted opportunities for the chemical upcycling of polyolefin waste,[11−13] stating the importance of processes that maximize selectivity and minimize energy costs. Reductive strategies toward heterogeneous catalytic cleavage of C−C bonds are a promising method of depolymerizing polyolefins under milder conditions than gasification or pyrolysis while minimizing loss of carbon to side products and coke formation.

Pt-based catalysts have been employed for the hydrogenolysis of PE at temperatures ranging from 250 to 385 °C and H_2 pressures ranging from 14 to 76 bar.[14−20] Recently, we demonstrated the high activity of ruthenium nanoparticles (NPs) supported on carbon (Ru/C) for the solvent-free hydrogenolysis of PE, PP, and mixtures of PE/PP waste under relatively mild conditions (200−250 °C, 20−50 bar H_2).[21,22] Ru/C was effective in depolymerizing PE and PP with molecular weights up to 54 kDa and 360 kDa, respectively, to produce liquid (C_5−C_{30}) yields of up to 45−68%, with the remaining products comprising gaseous hydrocarbons, predominantly methane, which has lower value and is a potent greenhouse gas. Other researchers have employed Ru-based catalysts on supports, including TiO_2, CeO_2, C, and NbO_5, for the hydrogenolysis of PE,[23−27] and mixtures containing polystyrene (PS),[28] further demonstrating the remarkable activity of this class of materials for C−C bond cleavage. By minimizing the loss of carbon toward CH_4, Ru-based catalysts could be promising materials for the depolymerization of polyolefin waste under mild conditions.

Several strategies can be implemented to suppress methane formation during C−C bond hydrogenolysis. Operating at high hydrogen pressures results in lower rates of terminal bond cleavage stemming from competitive adsorption of hydrogen atoms on the surface.[16] While hydrogen can be produced renewably through methods such as solar water-splitting,[29] the use of hydrogen incurs cost and increases the risk of safety hazards, including flammability and overpressurization.[30] Thus, it is more desirable to operate at lower hydrogen pressures to improve scalability and safety while reducing operating costs. Alternatively, bifunctional metal-acid sites promote the "ideal hydrocracking" of hydrocarbons, wherein central C−C bond cleavage is promoted through β-scission pathways.[31] Scheme 1 shows the proposed mechanism for ideal hydrocracking over PE (top) and PP (bottom), where metal sites catalyze hydrogenation/dehydrogenation and acid sites catalyze isomerization to produce carbocation intermediates. By promoting this bifunctional ideal hydrocracking pathway, we hypothesized that we could improve selectivity toward

https://doi.org/10.1021/acscatal.2c03596
ACS Catal. 2022, 12, 13969−13979

Table 1. Summary of Catalyst Characterization Obtained from TEM, H_2-TPR, NH_3-TPD, CO Pulse Chemisorption, and XAS

catalyst	Ru loading [wt %]	T_{max}, H_2-TPR [°C]	NH_3 adsorbed [μmol/g]	Ru dispersion [%]	d_p [nm][a]	d_p [nm][b]	d_p [nm][c]
Ru/Si-BEA	5.0	124	0	2.9	28	7.2 ± 5.5	2.9 ± 0.2
Ru/SiO_2	5.0	122	27	35	2.4	2.0 ± 0.9	2.2 ± 0.3
Ru/MWW	5.0	92	306	92	1.4	2.3 ± 0.4	NA
Ru/SIRAL30	5.0	83	180	70	1.2	1.3 ± 0.4	NA
Ru/SIRAL40HPV	5.0	785	1493	81	1.0	1.6 ± 0.5	NA
Ru/H-BEA	5.0	142	1409	32	2.5	2.4 ± 0.1	1.7 ± 0.3
Ru/FAU	5.0	81	1280	53	2.5	2.7 ± 1.2	2.4 ± 0.3

[a]Measured by CO pulse chemisorption. [b]Measured by TEM. [c]Obtained by extended X-ray absorption fine structure (EXAFS). Additional catalyst characterization data are provided in Figures S1−S6 in the Supporting Information.

nonterminal C−C bond cleavage, lowering methane formation and improving liquid yields.

Recently, Pt supported on acidic WO_x/ZrO_2 was employed as a bifunctional catalyst for the hydrocracking of PE at 250 °C and 30 bar H_2 for reaction times between 1 and 24 h, demonstrating the importance of metal-acid balance in promoting hydrocracking activity.[19,20] Ru is generally more active than Pt for C−C bond hydrogenolysis at the expense of higher methane formation but has not been largely studied for hydrocracking to maintain activity while reducing methane formation. Lee et al. found that under relatively harsh reaction conditions (300−350 °C), a Ru-modified zeolite with the faujasite (FAU) topology was highly active for the complete conversion of PE to methane in excess H_2, but this study mainly targeted methane production rather than liquid hydrocarbon production under milder conditions.[24]

Here, we investigated the role of acidic supports to improve the selectivity toward nonterminal C−C bond cleavage for Ru-based heterogeneous catalysts during PE and PP depolymerization. More specifically, we demonstrate that ruthenium NPs supported on acidic zeolites FAU (Si/Al 2.55) and Beta (BEA) (Si/Al 12.5) promote active and selective hydrocracking of PE and PP to produce liquid *n*-alkanes and *iso*-alkanes, respectively. We utilized different *operando* and *ex situ* characterization techniques, including microscopy, temperature-programmed desorption (TPD)/reduction, and X-ray absorption spectroscopy (XAS), as well as hydrogenolysis and hydrocracking reactivity experiments over a variety of supports to identify the key catalytic properties necessary to achieve high selectivity for polyolefin conversion to liquid alkanes under mild conditions. By identifying Ru dispersion and acid site density as key factors in promoting nonterminal C−C bond cleavage, this study identifies promising routes toward depolymerization and upcycling of PE and PP.

RESULTS AND DISCUSSION

Catalyst Characterization. A series of catalysts targeting a 5 wt % Ru loading were synthesized via incipient wetness impregnation and characterized with a suite of techniques, including transmission electron microscopy (TEM), temperature-programmed reduction with H_2 (H_2-TPR), temperature-programmed desorption of ammonia (NH_3-TPD), CO pulse chemisorption, powder X-ray diffraction (XRD), and XAS. Detailed procedures for the characterization and synthesis are provided in the Supporting Information. A summary of the characterization results is provided in Table 1. TEM images, histograms, XRD patterns, TPR profiles, and ammonia TPD profiles are provided in Figures S1−S6 in the Supporting Information.

These catalysts were chosen based on their varying acidity and structure for comparison against commercial 5 wt % Ru/C. The zeolites, FAU (Si/Al 2.55) and BEA (Si/Al 12.5), are microporous aluminosilicate materials and exhibit strong Brønsted acidity in their proton form. In addition to the strong acidity, they were selected due to their high surface areas and large pore sizes (~0.74 nm).[32] The pure-silica analogue (Si-BEA) was also selected to investigate the effect of the BEA structure without acidity. To investigate acidic but noncrystalline aluminosilicates, amorphous silica−alumina SIRAL catalysts were also selected, including SIRAL30 (Al_2O_3/SiO_2 70:30 wt %, 0.9 mL/g pore volume) and SIRAL40HPV (Al_2O_3/SiO_2 60:40 wt %, 1.5 mL/g pore volume). A delaminated zeolite with the MWW topology was synthesized to compare a crystalline Brønsted-acidic microporous aluminosilicate with an open two-dimensional (2D) structure. Amorphous silica (SiO_2, ~200 m^2/g) was selected as a control support with neither acidity nor crystalline structure.

CO pulse chemisorption was used to measure the Ru dispersion and estimate the nanoparticle diameter. The weight loading was calculated based on the loading of Ru precursor added during synthesis. Differences in the TPR profiles can be observed for the series of catalysts, as shown in further detail in Figure S3. The quantities of adsorbed ammonia from NH_3-TPD serve as an estimate of the quantity of acid sites, although this method cannot distinguish between Brønsted and Lewis acid sites.[33] Still, as expected, the highest adsorbed NH_3 quantities were observed for the strongly acidic catalysts, including Ru/H-BEA, Ru/FAU, Ru/SIRAL40HPV, and to a lesser extent, Ru/MWW and Ru/SIRAL30. The presence of strong Brønsted acid sites is well-established for the proton form of commonly used zeolites like FAU, BEA, and MWW.[34] While NH_3-TPD profiles only describe acid strength semi-quantitatively, the relatively high NH_3 desorption temperatures generally correlate with high Brønsted acid strength. NH_3-TPD profiles comparing Ru/BEA and Ru/SiO_2 (Figure S4) show that, in addition to having a higher quantity of acid sites, BEA exhibits a higher temperature of maximum NH_3 desorption (358 °C) compared to SiO_2 (188 °C). It is worth noting that the Ru/C catalyst also contains some acid sites (130 μmol NH_3/g), likely due to carboxylic acid functional groups present on the carbon support. Generally, the nanoparticle size distributions estimated from chemisorption measurements matched the measured average NP diameters from TEM and EXAFS, with the exception of Si-BEA, which indicated large (7.2 ± 5.5) NPs and poor Ru dispersion. The poor dispersion of ruthenium over the Si-BEA support (2.9%) compared to H-BEA (32%) could be due to the fact that acidic supports have been shown to aid in the dispersion of noble metal nanoparticles.[35] Still, the dispersion of Ru over SiO_2 (35%)

https://doi.org/10.1021/acscatal.2c03596
ACS Catal. 2022, 12, 13969−13979

was comparable to H-BEA, suggesting that other factors also affect the dispersion.

Catalyst Screening for Model PE and PP Hydrogenolysis/Hydrocracking. The initial catalyst screening reactions were performed with both PE and PP substrates (Tables S1−S3) at temperatures ranging from 200 to 250 °C and H_2 pressures ranging from 20 to 40 bar. Based on the high activity of ruthenium NPs supported on carbon and the precedent in the alkane hydrocracking literature for suppressing methane formation using a support containing Brønsted acid sites,[31] we tested a variety of ruthenium-based catalysts on supports with varying degrees of structure, acidity, and types of acid sites, as described in the section above. Reactions over PE (avg. M_w 4000 Da) were carried out over the series of catalysts in 25 mL Parr batch reactors at reaction conditions of 200 °C, 30 bar H_2, 600 RPM, over 16 h. The product selectivity toward liquid (C_5−C_{33}) and gaseous (C_1−C_5) hydrocarbons, as well as hydrogen conversion (mol %), is shown in Figure 1.

The liquid products consist of linear and branched alkanes ranging from C_6−C_{33}, and the gaseous hydrocarbons across all samples mainly comprise methane, ethane, and propane, with trace amounts of butane and pentane. The lack of unsaturated hydrocarbon products indicates that for every C−C bond cleaved, one molecule of hydrogen is consumed. Thus, tracking hydrogen conversion provides a critical metric for activity, enabling direct comparison of activity across catalysts and substrates and ensuring that the system is not hydrogen-starved. The most active catalysts for PE deconstruction on a basis of H_2 conversion were 5 wt % Ru on SiO_2, FAU, and H-BEA, with H_2 conversions of 71, 64, and 46%, respectively. Among the catalysts screened in Figure 1, the highest liquid yields were obtained over Ru/FAU (67%), Ru/H-BEA (51%), and Ru/SIRAL40HPV (46%). These supports all contain strong Brønsted acidity, consistent with the hypothesis that the Brønsted acid sites are promoting a hydrocracking mechanism that disfavors methane formation, giving rise to more central C−C bond cleavage toward liquid-range alkanes. Liquid yield increased from nonacidic Ru/SiO_2 (33%) to mildly acidic Ru/C (44%, Table S4) to strongly acidic Ru/FAU (67%), further supporting the trend of increasing liquid yield with increasing quantity of acid sites. Still, further comparison of structure and the quantity of acid sites at comparable H_2 conversions is necessary to develop relationships between acidity, structure, and C−C bond cleavage selectivity.

As shown in Figure 1a, at comparable H_2 conversions, Ru/FAU yields a higher liquid fraction compared to Ru/SiO_2. A physical mixture of Ru/SiO_2 and FAU results in lower activity and a liquid yield between that of Ru/SiO_2 and FAU, suggesting that the proximity of Ru/FAU is necessary to promote selectivity while maintaining activity. From the product distributions (Figure 1c−i), there is a significant quantity of branched hydrocarbons. The presence of branching is indicative of an ideal hydrocracking mechanism, where acid-catalyzed steps promote isomerization and subsequent β-scission of carbocation intermediates.[31] This mechanism promotes the scission of nonterminal C−C bonds, avoiding methane formation. The ideal hydrocracking mechanism differs from both the Haag−Dessau hydrocracking mechanism (which occurs solely over Brønsted acid sites) and the hydrogenolysis mechanism (which takes place solely over metal sites). To compare Ru/H-BEA and Ru/SiO_2 at similar H_2 conversions, shorter reaction times were carried out over Ru/SiO_2 to obtain data at lower conversions (Figure S9 and

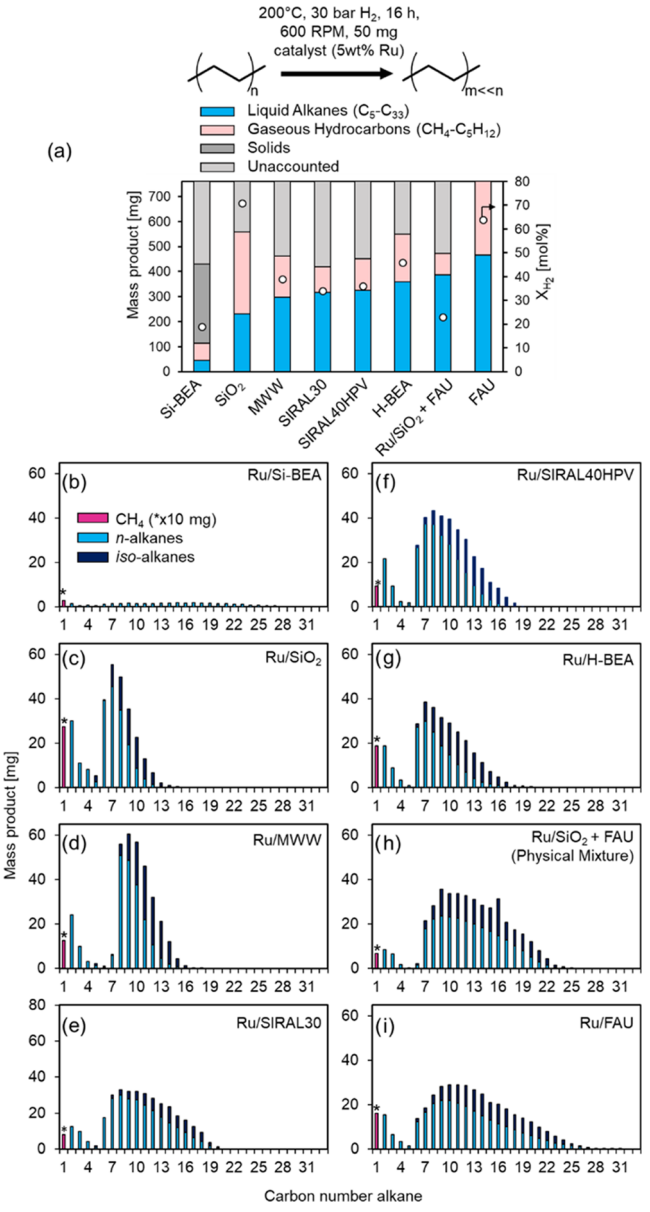

Figure 1. (a) Product yields for the reaction of PE (avg. M_w 4000 Da) over ruthenium-based catalysts (5 wt % Ru) on supports of varying acidity and structure. Reaction conditions: 200 °C, 16 h, 600 RPM, 30 bar H_2, 700 mg PE, 50 mg catalyst (50 mg Ru/SiO_2, 50 mg FAU for physical mixture). Tabulated values are given in Table S4, (b−i) liquid and gaseous product distributions for the reactions over Ru/Si-BEA, Ru/SiO_2, Ru/MWW, Ru/SIRAL30, Ru/SIRAL40HPV, Ru/H-BEA, physical mixture of Ru/SiO_2 and FAU (Ru/SiO_2 + FAU), and Ru/FAU. Methane products (pink, *) are in units of 10^1 mg to appear on the same plot. Representative gas chromatography−mass spectrometry (GC−MS) chromatograms are provided in Figures S7 and S8.

Table S5). Interestingly, at a conversion of ∼27%, the liquid yields for Ru/H-BEA and Ru/SiO_2 were similar (59 versus 63%, respectively). Generally, as hydrogen conversion increases, product distributions shift from higher carbon number alkanes to lower carbon number alkanes, and eventually, the products are completely in the gas phase as hydrogen is completely consumed. A representative time course study of this effect for PE conversion over Ru/H-BEA is shown in Figure S10. This representative time course

https://doi.org/10.1021/acscatal.2c03596
ACS Catal. 2022, 12, 13969−13979

demonstrates that under the conversions being compared, there is sufficient hydrogen present for the reaction to occur. It is worth noting that the activity and selectivity may change as a function of the transient hydrogen pressure in the reactions, further emphasizing the importance of comparing product distributions at similar hydrogen conversions.

FAU and BEA have both strong Brønsted acidity as well as a crystalline pore structure, which also may be responsible for the differences in selectivity and activity. To determine whether the three-dimensional (3D) micropores of the support are responsible for promoting selectivity, the reactivity for PE hydrogenolysis/hydrocracking was compared over Ru/H-BEA, Ru/Si-BEA, and Ru/MWW. As shown in Figure 1a, both activity and liquid yield increased from Ru/Si-BEA < Ru/MWW < Ru/H-BEA, with H_2 conversions increasing from 23% < 39% < 46 mol % H_2, and liquid yields increasing from 210 < 297 < 360 mg, respectively. The low activity of Ru/Si-BEA suggests that the zeolite BEA structure alone is insufficient to promote selectivity and activity effects. In contrast, Ru/MWW exhibited activity almost comparable to Ru/H-BEA, suggesting that either the Brønsted acidity or active site accessibility is an important factor in promoting activity.

A series of catalysts were then selected for further study with a PP substrate (avg. M_w 12,000 Da) at 215 °C, 30 bar H_2, over 16 h, as shown in Figure 2, with additional data in Table S6. Interestingly, despite having high activity for PE depolymerization, Ru/SiO_2, Ru/SIRAL30, and Ru/SIRAL40HPV showed little activity for PP depolymerization, yielding only small amounts of liquid product, as shown in Figure 2c,e,f, respectively. While the Ru/SIRAL30 catalyst showed some improvement over Ru/SiO_2 toward lowering methane formation, the overall liquid yields were low, yielding only trace alkane products in the liquid and wax range. In contrast, the Ru/H-BEA and Ru/FAU catalysts exhibited higher activity and selectivity toward liquid-range *iso*-alkanes, as shown in Figure 2g,i, respectively. The product distribution of Ru/H-BEA is narrower than that of Ru/FAU, suggesting either an intrinsic selectivity difference or a greater extent of reaction. To compare intrinsic selectivity, reactions were carried out at shorter reaction times over the Ru/H-BEA catalyst to compare product distributions at a constant hydrogen conversion (i.e., constant total number of C−C bond cleaved). Figure S13 and Table S7 show the product distribution and quantities for PP cleavage as a function of time over Ru/H-BEA between 12 and 16 h. At 12 h, the liquid yield is approximately 56% over Ru/H-BEA compared to 52% over Ru/FAU at hydrogen conversion levels of 10 and 9%, respectively. This demonstrates that both zeolites generate similar selectivity and product distributions, with BEA featuring a slightly narrower product distribution centered around C_6−C_8 compared to a distribution centered around C_8−C_{11} over FAU.

For PP depolymerization, a physical mixture of Ru/SiO_2 and FAU performed similarly to Ru directly supported on FAU (Ru/FAU), with similar liquid yields and only a slight preference for suppressed methane formation and slightly narrower product distribution over the directly supported material. This suggests that, while metal-acid site proximity does help suppress methane formation, the difference between the physical mixture and directly supported material is less significant than over the model PE.

In a recent study, Zichittella et al. reported that zeolite ZSM-5 alone was active for PE and PP hydrocracking at 250 °C over

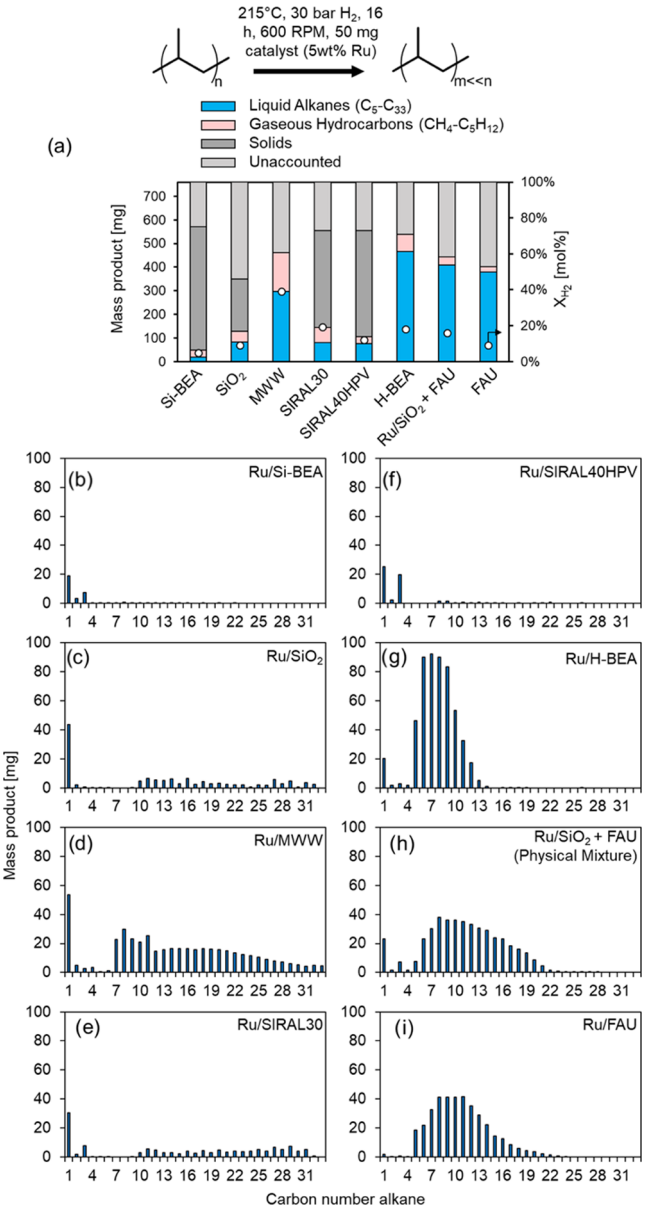

Figure 2. (a) Product yields for the deconstruction of PP (avg. M_w 12,000 kDa) over Ru/Si-BEA, Ru/SiO_2, Ru/MWW, Ru/SIRAL30, Ru/SIRAL40HPV, Ru/H-BEA, physical mixture of Ru/SiO_2 and FAU, and Ru/FAU; (b−i) liquid (*iso*-alkanes) and gaseous product distributions for the data in panel (a). Reaction conditions: 215 °C, 16 h, 30 bar H_2, 600 RPM, 700 mg PP, 50 mg (50 mg each Ru/SiO_2, FAU for physical mixture). Tabulated values are given in Table S6. Representative GC−MS chromatograms are provided in Figures S11 and S12.

20 h in 40 bar H_2, although the addition of Co nanoparticles promoted stability and selectivity.[36] To rule out the possibility that FAU and BEA supports alone are contributing to the high hydrocracking activity under the reaction conditions reported here, a series of control reactions were performed in the absence of ruthenium nanoparticles. As shown in Figure S14 and Table S8, H-FAU and H-BEA are nearly inactive for hydrocracking of PE or PP at 200 °C and 215 °C, respectively, over 16 h in 30 bar H_2. Trace amounts of gaseous hydrocarbons C_1−C_6 were produced, and minimal liquid products were formed, with the remainder being unreacted solids. This is consistent with the results of Liu et al., who

https://doi.org/10.1021/acscatal.2c03596
ACS Catal. 2022, 12, 13969−13979

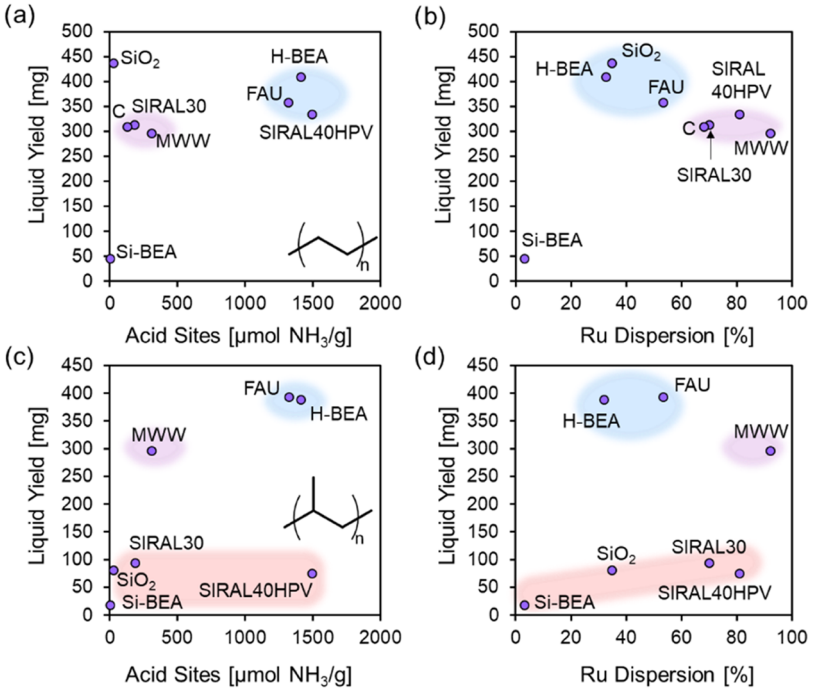

Figure 3. (a) Liquid yield as a function of the quantity of acid sites estimated by NH_3-TPD (μmol NH_3/g) for PE (avg. M_w 4000 Da) deconstruction at 200 °C, 30 bar H_2, 16 h, 700 mg PE, 600 RPM, over 5 wt % Ru-based catalysts on various supports (50 mg) at hydrogen conversions between 20 and 35%; (b) liquid yield as a function of Ru dispersion (%) for the reaction conditions given in panel (a); (c) liquid yield as a function of the quantity of acid sites estimated by NH_3-TPD (μmol NH_3/g) for PP (avg. M_w 12,000 Da) deconstruction at 215 °C, 30 bar H_2, 16 h, 700 mg PP, 600 RPM, over 5 wt % Ru-based catalysts on various supports (50 mg) at hydrogen conversions between 6 and 14%; (d) liquid yield as a function of Ru dispersion (%) for the reaction conditions given in panel (c).

observed minimal activity for zeolite FAU at 250 °C over 2 h in 30 bar H_2.[20] From this, we could conclude that the zeolite supports alone were not contributing significantly to the C−C bond cleavage activity, further suggesting that cooperation with the metal sites is important.

The Ru/FAU catalyst was then employed for the depolymerization of additional substrates, including a PE standard reference material from NIST (SRM 1475), a low-density PE (LDPE) post-consumer plastic bottle, a PP post-consumer centrifuge tube, and a higher-molecular-weight PP (avg. M_w 340,000 kDa). The Ru/FAU was able to catalyze the depolymerization of each of these substrates to liquid and gaseous products under reaction conditions ranging from 225 to 250 °C, at times between 2 and 24 h and H_2 pressures from 20 to 40 bar, as shown in Figure S15 and Table S9, with additional details on product quantification and analysis with a representative reaction provided in Figure S16. The ability of the catalyst to depolymerize a range of well-characterized substrates and post-consumer PE and PP is a promising step toward valorizing realistic waste streams.

Relationship of Catalytic Performance to Acid Site Quantity and Ru Dispersion. To relate the quantity of acid sites (estimated by NH_3-TPD) and Ru dispersion (estimated by CO pulse chemisorption) to catalyst selectivity for PE and PP reactions, liquid yields were plotted as a function of the quantity of acid sites and dispersion across the series of catalysts shown in Figures 1 and 2. This relationship, shown in Figure 3, used data at similar hydrogen conversions to decouple the intrinsic selectivity from the extent of reaction, as higher activity and thus higher hydrogen conversion generally result in lower liquid yields due to cascade C−C bond cleavage reactions, as shown over Ru/H-BEA in Figure S10 for PE and Figure S13 for PP. From Figure 3a, it can be observed that there is a general trend toward improved liquid yields with increasing acid site count for reactions over PE (avg. M_w 4000 Da, 200 °C). The exception is the high liquid yield over Ru/SiO_2, which has little to no acidity, yet at the same conversion as the other catalysts, exhibits relatively high liquid yields. A stronger correlation is apparent in Figure 3b, where there appears to be a maximum liquid yield at an intermediate ruthenium dispersion of ca 40%, beyond which the selectivity toward liquid products begins to decrease. The highest liquid yields at *iso*-H_2 conversion for PE depolymerization occur over Ru/SiO_2, Ru/H-BEA, Ru/FAU, and to a lesser extent, Ru/MWW, suggesting that an optimal dispersion promotes internal C−C bond cleavage. In a study of Ru/Al_2O_3 catalysts for propane and *n*-butane hydrogenolysis, Bond et al. found that methane selectivity decreased with increasing dispersion of Ru and that the highly dispersed Ru catalysts facilitated a 2,3-adsorbed C_4 intermediate, giving way to ethane formation.[37] Coq et al. studied the impact of Ru dispersion on the hydrogenolysis of a series of linear and branched hydrocarbons between 150 and 220 °C and found that large particles of Ru promoted so-called "deep hydrogenolysis," where rates of alkane desorption are low, resulting in high amounts of methane formation from surface-bound alkanes.[38]

Interestingly, for reactions over PP (avg. M_w 12,000 Da, 215 °C), there is a clear and strong positive correlation between liquid yield and the quantity of acid sites, as shown in Figure 3c. Ru/FAU and Ru/H-BEA catalysts were the best performing in terms of liquid yields; however, Ru/SiO_2, which performed well for PE reactions, was barely active and produced waxy and solid products at similar H_2 conversions to those for the zeolites FAU and H-BEA. The exception to the

https://doi.org/10.1021/acscatal.2c03596
ACS Catal. 2022, 12, 13969−13979

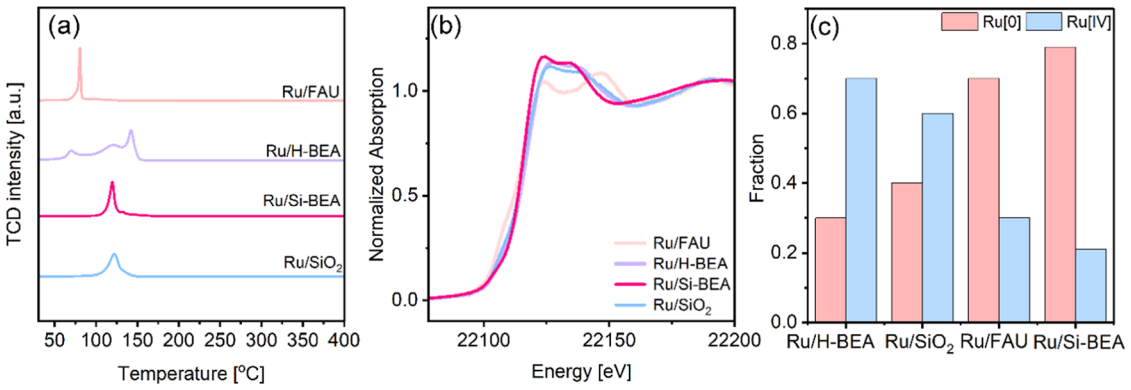

Figure 4. (a) H_2-TPR profiles of Ru/FAU, Ru/H-BEA, Ru/Si-BEA, and Ru/SiO_2; (b) *ex situ* Ru K-edge XANES for the Ru-supported catalysts; and (c) XANES-linear combination fits (LCF). EXAFS analysis and linear combination fitting results are presented in Figure S22 and Tables S10–S12 of the Supporting Information.

trend is Ru/SIRAL40HPV, which exhibited low selectivity toward liquid-range products at approximately the same hydrogen conversion. From the NH_3-TPD curves in Figure S4, its distribution of strength of acid sites, estimated by the desorption temperature profile, is much wider than that of Ru/H-BEA and Ru/FAU, suggesting that the quantity of acid sites alone is not enough of a predictor of activity for PP, but that the structure of the support and strength of the acid sites also play a key role. Unlike PE reactions, over PP, the ruthenium dispersion did not correlate with liquid yield, suggesting that acidity plays a more dominant role for the deconstruction of PP (Figure 3d). As shown in Figure S17, the relationship between the quantity of acid sites (μmol NH_3/g) and moles of CH_4 produced per mole of H_2 consumed is fairly constant across all of the supports studied for PE; however, for PP, the moles of CH_4 produced per mole of H_2 consumed decreases significantly as the quantity of acid sites (μmol NH_3/g) of the support increases, further suggesting that the acidity shifts away from the hydrogenolysis mechanism which favors methanation.

The relationship between the quantity of acid sites and liquid yields is stronger for the reactions over PP than for PE. Direct comparison of these two substrates is difficult due to the different temperatures of reaction and the different molecular weights and physical properties of the two model polymers. Still, there are a few reasons why the correlation between the quantity of acid sites and liquid yields is much stronger for PP. One reason could be that at lower temperatures required for PE deconstruction, the Brønsted acid-catalyzed hydrocracking pathway is less dominant. To test this, PE reactions were carried out over lower reaction times at 215 °C to compare selectivity over Ru/SiO_2 and Ru/H-BEA at the same H_2 conversion. Reactions of PE over Ru/SiO_2 and Ru/H-BEA at 215 °C, 4 h, and 30 bar H_2 (Figure S18) resulted in H_2 conversions of 11 and 24%, and liquid yields of 64 and 41%, respectively. The fraction of branched alkanes was 11% over Ru/SiO_2 compared to 24% over Ru/H-BEA, further suggesting that acid-catalyzed isomerization steps are favored at higher temperatures.

Another hypothesis is that the branches on the PP substrate facilitate the hydrocracking mechanism by providing substituted C–C bonds to stabilize carbocation intermediates generated by acid sites. As shown in Scheme 1, Ru metal sites first catalyze dehydrogenation of PE or PP to a surface olefinic intermediate, which are then protonated by the Brønsted acid site. In the case of PE, the acid catalyzes rearrangement to stabilize the carbocation intermediate, followed by β-scission and then regeneration of the Brønsted acid site and reduction of the cleaved products on the metal site. In the case of PP, the carbocation intermediate is stabilized by methyl branches on the substrate, promoting the transition state required for β-scission across the C–C bond to produce cleaved intermediates, which is then hydrogenated by hydrogen activated on the Ru metal surface. Thus, over PP, the carbocation generated in the second step does not require an additional acid-catalyzed isomerization step to stabilize the intermediate and promote β-scission, suggesting that isomerization plays a critical role in determining the rate of reaction for PE hydrocracking in the presence of Brønsted acid supports. The role of the isomerization step could also help explain why the acid/noble metal proximity was less important for PP hydrocracking compared to PE hydrocracking because for PP, the carbocation intermediate is already stabilized by the methyl branches.

Role of Ru Nanoparticle Reducibility and XAS Analysis. From the correlations between the quantity of acid sites and dispersion for PE hydrocracking/hydrogenolysis shown in Figure 3, it remains unclear how the support changes the formation of the nanoparticles and the oxidation state of ruthenium after reduction, as well as the structure and active state of the ruthenium under reaction conditions. For this information, we turned toward *ex situ* and *operando* XAS measurements and performed modeling of the EXAFS data at the Ru K-edge to determine the effect of support on the formation and average size of Ru NPs and the *in situ* chemical state and stability of the ruthenium NPs during hydrogenolysis. XAS correlations with activity are provided in Figures S19 and S20, and the methods and analysis are provided in Figures S21–S35 and Tables S10–S19 in the Supporting Information.

H_2-TPR of Ru nanoparticles supported on FAU, H-BEA, Si-BEA, and SiO_2 (Figure 4a) profiles depend on the support. The temperature of maximum H_2 uptake is similar for Ru/Si-BEA (124 °C) and Ru/SiO_2 (122 °C), but there is an increase over Ru/H-BEA (142 °C) and a decrease over Ru/FAU (81 °C). The selected catalysts shown in Figure 4a also show differences in the Ru K-edge X-ray absorption near-edge structure (XANES) after drying and subsequent reduction at 400°C (Figure 4b), suggesting that there are variations in the Ru local structure. XANES-linear combination analysis (LCA) of these *ex situ* catalysts shows both metallic and oxidic species,

https://doi.org/10.1021/acscatal.2c03596
ACS Catal. 2022, 12, 13969–13979

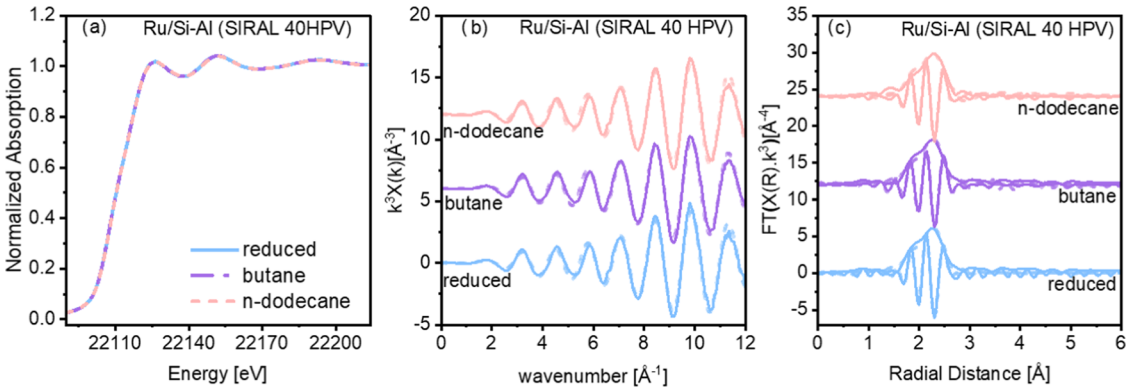

Figure 5. Ru K-edge (a) XANES, (b) EXAFS data and fits in *k* space, and (c) FT-EXAFS (*R* space) for Ru/SIRAL40HPV after reduction and hydrogenolysis in butane and *n*-dodecane collected at 200°C, illustrating the structural changes due to changes in the gas environment: reaction (butane or *n*-dodecane and hydrogen). Experimental EXAFS (solid lines) and fits (dashed lines) are compared in panel (a) *k* and panel (b) *R* space (with imaginary components plotted as dashed lines). Fits were performed using an *r* range of 1.0−3.0 Å and a *k* range of 3.0−13.0 $Å^{-1}$.

with their estimated fractions shown in Figures S23 and S24. The best fit results of the EXAFS modeling along with XANES-LCA analysis indicate that for this set, Ru/H-BEA contains the highest oxidic fraction (Figure 4c and Tables S10−S12).

The catalytic activity for the deconstruction of PE can be correlated to the $Ru^{[0]}$ fraction. As shown in Figure S19a, across the series of catalysts under the same reaction conditions (200 °C, 16 h, 30 bar H_2), the conversion of H_2 increases with increasing fraction of $Ru^{[0]}$ as measured by XANES. The quantities of gaseous products also increase with the fraction of $Ru^{[0]}$ (Figure S19b), as the quantities of gaseous products are coupled to H_2 conversion. Interestingly, for reactions over PP (215 °C, 16 h, 30 bar H_2), there appears to be no correlation between hydrogen conversion nor gaseous product yields with the $Ru^{[0]}$ fraction (Figure S19c,d). Across the catalysts studied with XANES, the $Ru^{[0]}$ fraction reaches a maximum at a dispersion of 50% (Ru/FAU), as shown in Figure S20. This could explain the ideal dispersion of ∼40−50% for PE deconstruction activity and selectivity.

The oxidation state of Ru on a series of as-prepared catalysts was also tracked using *in situ* temperature-programmed reduction-XANES in hydrogen. The shift from the oxidic ruthenium to metallic ruthenium across the series of catalysts is shown in Figures S25−S27. TPR-XANES results agree with H_2-TPR, which indicates that the temperature of maximum reduction is dependent on the support (Figure S26 and Table S13). We note that Ru reduction on the SIRALS was incomplete by 500°C (Figures S26 and S28). These catalysts exhibit similar selectivity to that of the Ru/H-BEA for PE hydrogenolysis but exhibit lower overall conversions under the same reaction conditions, suggesting that the reducibility and Ru speciation are not the only factors driving the hydrogenolysis process. EXAFS modeling on the fully reduced Ru NPs was performed to extract average particle size using the hemispherical method (detailed in the Supporting Information, Figure S29). As shown in Table 1, the average Ru NP size ranges from 1.7 to 2.9 nm, consistent with the particle sizes obtained from TEM images (Table S14). Evaluation of the structural disorder of the Ru NPs to address the appropriate preactivation condition steps was performed by modeling temperature dependence on the metallic Ru particles in a hydrogen environment after reduction (discussed in detail in the Supporting Information, Figures S30−S32 and Tables S15, S16). Collectively, the *in situ* temperature reduction process showed the role of metal−support interactions and the effect of the support on the formation of ruthenium NPs.

Ru K-edge *ex situ* XAS was also used to probe changes in the catalyst before and after PE hydrogenolysis. For Ru/H-BEA, an increase in metallic content is observed after PE hydrogenolysis (Figure S33 and Table S17; detailed description in the Supporting Information). *In situ* hydrogenolysis of model alkanes (*n*-butane, *n*-dodecane) was carried out to track the Ru speciation in real time during the hydrogenolysis reactions in flowing hydrogen at reaction temperature. Ru/SIRAL40HPV, which exhibited high performance for PE hydrogenolysis, was chosen as a model catalyst for the *operando* polyolefin hydrogenolysis studies. The EXAFS features on this catalyst after *n*-butane and *n*-dodecane hydrogenolysis are similar compared to the reduced Ru/SIRAL40HPV (Figure 5). EXAFS modeling indicated that Ru/SIRAL40HPV catalyst is unchanged under reaction conditions (Table S18), suggesting that both *n*-butane and *n*-dodecane serve as equivalent probe molecules. Additionally, the other seven catalysts studied show no differences in the Ru speciation under *n*-butane hydrogenolysis in flowing hydrogen (10 mL/min) at 200 °C (Figures S34, S35 and Table S19).

CONCLUSIONS AND OUTLOOK

Bifunctional heterogeneous catalysts containing metal sites (ruthenium nanoparticles) supported on Brønsted acids (zeolites FAU and BEA) are effective catalysts for the reductive cleavage of C−C bonds in polyolefins (PE and PP) to produce high yields of liquid alkanes, showing improvement over nonacidic supports such as silica and mildly acidic carbon. Reactivity data across catalysts with varying quantities of acid sites and support structure suggest that Brønsted-acidic supports promote an ideal hydrocracking mechanism, where carbocation intermediates favor the formation of transition states for nonterminal C−C bond cleavage, thus preventing loss of carbon due to methane formation. The ruthenium nanoparticle dispersion, characterized by CO pulse chemisorption, was dependent on the support and revealed an optimal dispersion of around 40−50% at a 5 wt % Ru loading for high selectivity toward PE hydrogenolysis, which also corresponds to a maximum in the fraction of $Ru^{[0]}$ as measured by XANES. *In situ* reduction of Ru-based catalysts revealed an increase in reduction temper-

https://doi.org/10.1021/acscatal.2c03596
ACS Catal. 2022, 12, 13969−13979

ature of about 50 °C for the formation of nanoparticles supported on SiO_2 to H-BEA, consistent with H_2-TPR measurements. *Operando* EXAFS of hydrogenolysis reactions using model PE (*n*-butane, *n*-dodecane) in flowing hydrogen at reaction temperature revealed that metallic Ru is the active species for C−C bond hydrogenolysis and is largely unchanged with varying supports, supporting the hypothesis that acidity and dispersion, rather than Ru reducibility, are the dominant factors in determining selectivity and activity. EXAFS studies also confirmed the stability of the catalysts under reaction conditions, indicating promise for this class of material for the selective conversion of plastic waste to processable liquid alkanes.

MATERIALS AND METHODS

Materials. Polymeric substrates, including PE (avg. M_w ~4000 Da), PP (avg. M_w ~12,000 Da), and PP (avg. M_w ~340,000 Da), were obtained from Sigma-Aldrich and are described in the Supporting Information, with additional details provided in Tables S1−S3. Zeolite FAU (H^+ form, 730 m^2/g surface area, SiO_2/Al_2O_3 5.1) was obtained from Zeolyst International (CBV400, P#400054002618). Zeolite BEA (NH_4^+, 680 m^2/g, SiO_2/Al_2O_3 25) was obtained from Zeolyst International and was calcined at 550 °C for 5 h to convert to acid form (H-BEA) prior to the reaction. Silicon dioxide, (fumed, Lot#MKBH4409V) was obtained from Sigma-Aldrich. Ruthenium on carbon support (5 wt % Ru, powder) was obtained from Sigma-Aldrich. Acidic silica−alumina supports (SIRAL30 and SIRAL40HPV) were obtained from Sasol. Zeolite Si-BEA was synthesized according to the literature.[39] MWW was prepared according to the literature,[40] as described in the Supporting Information.

Catalyst Synthesis. Ruthenium nanoparticles (5 wt %) supported on zeolites FAU and BEA were synthesized via incipient wetness impregnation of ruthenium (III) nitrosyl nitrate. The supports were calcined at 500 °C for 3 h prior to impregnation. The incipient wetness point was determined by adding nanopure water dropwise to the support and mixing with mortar and pestle until the catalyst adopted a mud-like consistency. The ruthenium(III) nitrosyl nitrate was then dissolved completely in nanopure water and added to the support dropwise and mixed with a mortar and pestle. The catalyst was then dried overnight at 110 °C. The catalyst was then reduced in flowing hydrogen (100 mL/min) at 400 °C for 3 h at a heating rate of 3 °C/min. Ruthenium nanoparticles (5 wt %) supported on SiO_2, SIRAL30, SIRAL40HPV, and MWW were synthesized via incipient wetness impregnation of ruthenium (III) nitrosyl nitrate according to the procedure described above for the FAU and H-BEA-supported catalysts. After impregnation and drying, the catalysts were reduced in flowing hydrogen (100 mL/min) at 400 °C for 3 h at a heating rate of 3 °C/min. 5 wt % Ru/Si-BEA was synthesized via wetness impregnation of ruthenium (III) nitrosyl nitrate. First, the catalyst was calcined in a muffle furnace at 580 °C for 6 h at a heating rate of 1 °C/min and then cooled to room temperature. Because of the lower pore volume, two impregnations were performed. Half of the solution was then added dropwise to the support to the point of incipient wetness and mixed. The catalyst was then allowed to dry overnight at 110 °C. After cooling, the rest of the precursor solution was added to the catalyst to reach the point of incipient wetness again. The catalyst was then dried again overnight at 110 °C and then reduced in flowing hydrogen (100 mL/min) at 400 °C for 3 h at a heating rate of 3 °C/min.

Catalyst Characterization and XAS Measurements. Details for catalyst characterization, including transmission electron microscopy (TEM), X-ray diffraction (XRD), temperature-programmed reduction (H_2-TPR), CO chemisorption titration, and ammonia temperature-programmed desorption (NH_3-TPD), and CO temperature-programmed desorption, are described in detail in the Supporting Information. *Ex situ* and *in situ/operando* X-ray absorption spectroscopy (XAS) experiments at the Ru K-edge were carried out at the Stanford Synchrotron Radiation Light Source of the SLAC National Accelerator Laboratory. Detailed experimental procedures and beamline configuration, as well as details of the *operando* setup, are provided in the Supporting Information.

Polyolefin Hydrogenolysis. Hydrogenolysis of PE and PP was carried out in 25 mL Parr pressurized stainless steel reactors equipped with magnetic stirring. In a typical reaction, the plastic substrate (PE powder or PP beads) was added directly to the reactor and mixed with the catalyst and a magnetic stir bar. PE powder (avg. M_w 4000 Da) and PP beads (avg. M_w 12,000 Da) were used as is, and PP beads (avg. M_w 340,000 Da) were cut to pieces approximately 5 mm in diameter before adding to the reactor. The reactor was then sealed, purged at least three times with hydrogen gas, and then pressurized to the specified hydrogen pressure at room temperature. The reactor was then placed in an aluminum block and heated to the reaction temperature over the course of 40 min with a temperature controller accurate to ±1 °C. After the specified reaction time (including the heating time of ~40 min), the reactor was quenched in an ice bath. After cooling to room temperature, the final pressure was recorded, and the headspace was collected in a gas bag and analyzed with gas chromatography (GC) equipped with a flame ionization detector (FID) and a thermal conductivity detector (TCD) to quantify C_1−C_5 hydrocarbons and H_2, respectively. Helium was used as the carrier gas for TCD, and the negative hydrogen peak was flipped for integration. Calibration curves for mole fractions of gaseous products were obtained by flowing varying known ratios of each gas at atmospheric pressure through mass flow controllers feeding directly to the GC-TCD. Liquid products (C_6−C_{30}) were dissolved in acetone, identified with GC−MS, and quantified with GC-FID using 1,3,5-tri-tertbutyl benzene as an external standard. Pentanes (C_5) and trace amounts of hexanes (C_6) can exist in both gas and liquid phases; thus, the total quantity of pentanes and hexanes is summed from the analysis of both the headspace and liquid products. For reactions with insoluble solid products, the solids were weighed, and the mass of the catalyst was subtracted to record the solid product yield. The missing mass balances for each reaction may be attributed to unrecovered solids, gaseous products, or soluble waxes that are undetectable by GC. Each experiment was repeated and analyzed in toluene solvent to identify peaks that overlap with the solvent. A scheme detailing the identification and quantification of the iso-alkane products from PP hydrogenolysis is provided in the Supporting Information in our previous study.[22]

The conversion of hydrogen is a metric for C−C bond cleavage activity, as one molecule of H_2 is consumed for each C−C bond cleaved. Hydrogen conversion is defined by eq 1

$$X_{H_2}[\text{mol \%}] = 1 - \frac{\text{mol } H_2 \text{ after reaction}}{\text{initial mol } H_2} \quad (1)$$

https://doi.org/10.1021/acscatal.2c03596
ACS Catal. 2022, 12, 13969−13979

Liquid yield is defined by eq 2

$$Y_{liquid}[\text{mass \%}] = \frac{\text{mass hydrocarbons } (C_6 - C_{33}) \text{ after reaction}}{\text{initial mass PE or PP} + \text{initial mass } H_2} \quad (2)$$

Gaseous yield is defined by eq 3

$$Y_{gas}[\text{mass \%}] = \frac{\text{mass hydrocarbons } (C_1 - C_6) \text{ after reaction}}{\text{initial mass PE or PP} + \text{initial mass } H_2} \quad (3)$$

The "unaccounted" mass was calculated by subtracting the masses of liquid and gaseous products and recovered solids from the initial mass of hydrogen and PE or PP.

■ ASSOCIATED CONTENT

Supporting Information

The Supporting Information is available free of charge at https://pubs.acs.org/doi/10.1021/acscatal.2c03596.

Experimental details, additional catalyst characterization, supporting experiments, and X-ray adsorption spectroscopy methods and analysis (PDF)

■ AUTHOR INFORMATION

Corresponding Author

Yuriy Román-Leshkov − *Department of Chemical Engineering, Massachusetts Institute of Technology, Cambridge, Massachusetts 02139, United States;* orcid.org/0000-0002-0025-4233; Email: yroman@mit.edu

Authors

Julie E. Rorrer − *Department of Chemical Engineering, Massachusetts Institute of Technology, Cambridge, Massachusetts 02139, United States;* orcid.org/0000-0003-4401-8520

Amani M. Ebrahim − *SLAC National Accelerator Laboratory, Menlo Park, California 94025, United States; BOTTLE Consortium, Golden, Colorado 80401, United States*

Ydna Questell-Santiago − *Department of Chemical Engineering, Massachusetts Institute of Technology, Cambridge, Massachusetts 02139, United States*

Jie Zhu − *Department of Chemical Engineering, Massachusetts Institute of Technology, Cambridge, Massachusetts 02139, United States*

Clara Troyano-Valls − *Department of Chemical Engineering, Massachusetts Institute of Technology, Cambridge, Massachusetts 02139, United States*

Arun S. Asundi − *SLAC National Accelerator Laboratory, Menlo Park, California 94025, United States; BOTTLE Consortium, Golden, Colorado 80401, United States;* orcid.org/0000-0003-0333-6784

Anna E. Brenner − *Department of Chemical Engineering, Massachusetts Institute of Technology, Cambridge, Massachusetts 02139, United States;* orcid.org/0000-0003-3669-2515

Simon R. Bare − *SLAC National Accelerator Laboratory, Menlo Park, California 94025, United States; BOTTLE Consortium, Golden, Colorado 80401, United States*

Christopher J. Tassone − *SLAC National Accelerator Laboratory, Menlo Park, California 94025, United States; BOTTLE Consortium, Golden, Colorado 80401, United States*

Gregg T. Beckham − *Renewable Resources and Enabling Sciences Center, National Renewable Energy Laboratory, Golden, Colorado 80401, United States; BOTTLE Consortium, Golden, Colorado 80401, United States;* orcid.org/0000-0002-3480-212X

Complete contact information is available at: https://pubs.acs.org/10.1021/acscatal.2c03596

Notes

The authors declare no competing financial interest.

■ ACKNOWLEDGMENTS

Funding was provided by the U.S. Department of Energy, Office of Energy Efficiency and Renewable Energy, Advanced Manufacturing Office (AMO), and Bioenergy Technologies Office (BETO). This work was performed as part of the Bio-Optimized Technologies to keep Thermoplastics out of Landfills and the Environment (BOTTLE) Consortium and was supported by AMO and BETO under Contract DE-AC36-08GO28308 with the National Renewable Energy Laboratory (NREL), operated by Alliance for Sustainable Energy, LLC. The BOTTLE Consortium includes members from MIT, funded under Contract DE-AC36-08GO28308 with NREL. Use of the Stanford Synchrotron Radiation Light Source, SLAC National Accelerator Laboratory is supported by the Department of Energy, AMO and BETO funding programs under agreements 37496 and 37430 at SLAC National Accelerator Laboratory, under contract DE-AC02-76SF00515. *In situ/Operando* XAS setup is made possible by Co-ACCESS that is supported by the U.S. Department of Energy, Office of Basic Energy Sciences, Geoscience and Biosceince Divison. J.E.R. is also supported by an Arnold O. Beckman Postdoctoral Fellowship. Y.Q.-S. acknowledges support of the SNSF Swiss Postdoctoral Fellowship (SPF), grant number P2ELP2_187960. The authors thank Griffin Drake, Dr. Bing Yan, and Dr. Guido Zichittella for useful discussion, Dr. Jennifer Lewis for providing synthesized Si-BEA, and Joel Miscall for providing plastic substrate materials. We also thank Dr. Kathryn Beers and Dr. Sara Orski for providing NIST PE standard reference materials. A.M.E. thanks Dr. Adam Hoffman and Dr. Jorge Perez-Aguilar for assistance with the *in situ/operandon*-dodoecane setup at XAS BL 2-2. The views expressed in the article do not necessarily represent the views of the DOE or the U.S. Government.

■ REFERENCES

(1) Geyer, R.; Jambeck, J. R.; Law, K. L. Production, use, and fate of all plastics ever made. *Sci. Adv.* **2017**, *3*, No. e1700782.

(2) Hong, M.; Chen, E. Y. X. Future directions for sustainable polymers. *Trends Chem.* **2019**, *1*, 148−151.

(3) Nicholson, S. R.; Rorrer, N. A.; Carpenter, A. C.; Beckham, G. T. Manufacturing energy and greenhouse gas emissions associated with plastics consumption. *Joule* **2021**, *5*, 673−686.

(4) IHS Markit. *Chemical Economics Handbook (CEH): Plastics Recycling*; IHS Markit, 2020.

(5) Milbrandt, A.; Coney, K.; Badgett, A.; Beckham, G. T. Quantification and evaluation of plastic waste in the United States. *Resour., Conserv. Recycl.* **2022**, *183*, No. 106363.

(6) Nicholson, S. R.; Rorrer, J. E.; Singh, A.; Konev, M. O.; Rorrer, N. A.; Carpenter, A. C.; Jacobsen, A. J.; Román-Leshkov, Y.; Beckham, G. T. The critical role of process analysis in chemical

recycling and upcycling of waste plastics. *Annu. Rev. Chem. Biomol. Eng.* **2021**, *13*, 14.1−14.24.
(7) Vollmer, I.; Jenks, M. J. F.; Roelands, M. C. P.; White, R. J.; van Harmelen, T.; de Wild, P.; van der Laan, G. P.; Meirer, F.; Keurentjes, J. T. F.; Weckhuysen, B. M. Beyond mechanical recycling: giving new life to plastic waste. *Angew. Chem., Int. Ed.* **2020**, *59*, 15402−15423.
(8) Serrano, D. P.; Aguado, J.; Escola, J. M. Developing advanced catalysts for the conversion of polyolefinic waste plastics into fuels and chemicals. *ACS Catal.* **2012**, *2*, 1924−1941.
(9) Anuar Sharuddin, S. D.; Abnisa, F.; Wan Daud, W. M. A.; Aroua, M. K. A review on pyrolysis of plastic wastes. *Energy Convers. Manage.* **2016**, *115*, 308−326.
(10) Kunwar, B.; Cheng, H. N.; Chandrashekaran, S. R.; Sharma, B. K. Plastics to fuel: a review. *Renewable Sustainable Energy Rev.* **2016**, *54*, 421−428.
(11) Ellis, L. D.; Rorrer, N. A.; Sullivan, K. P.; Otto, M.; McGeehan, J. E.; Román-Leshkov, Y.; Wierck, N.; Beckham, G. T. Chemical and biological catalysts for plastics recycling and upcycling. *Nat. Catal.* **2021**, *4*, 539−556.
(12) Jehanno, C.; Alty, J. W.; Roosen, M.; De Meester, S.; Dove, A. P.; Chen, E. Y.; Leibfarth, F. A.; Sardon, H. Critical advances and future opportunities in upcycling commodity polymers. *Nature* **2022**, *603*, 803−814.
(13) Mark, L. O.; Cendejas, M. C.; Hermans, I. The use of heterogeneous catalysis in the chemical valorization of plastic waste. *ChemSusChem* **2020**, *13*, 5808−5836.
(14) Celik, G.; Kennedy, R. M.; Hackler, R. A.; Ferrandon, M.; Tennakoon, A.; Patnaik, S.; LaPointe, A. M.; Ammal, S. C.; Heyden, A.; Perras, F. A.; Pruski, M.; Scott, S. L.; Poeppelmeier, K. R.; Sadow, A. D.; Delferro, M. Upcycling single-use polyethylene into high-quality liquid products. *ACS Cent. Sci.* **2019**, *5*, 1795−1803.
(15) Calemma, V.; Peratello, S.; Perego, C. Hydroisomerization and hydrocracking of long chain n-alkanes on Pt/amorphous SiO2−Al2O3 catalyst. *Appl. Catal., A* **2000**, *190*, 207−218.
(16) Kots, P. A.; Vance, B. C.; Vlachos, D. G. Polyolefin plastic waste hydroconversion to fuels, lubricants, and waxes: a comparative study. *React. Chem. Eng.* **2021**, *7*, 41−54.
(17) Tennakoon, A.; Wu, X.; Paterson, A. L.; Patnaik, S.; Pei, Y.; LaPointe, A. M.; Ammal, S. C.; Hackler, R. A.; Heyden, A.; Slowing, I. I.; Coates, G. W.; Delferro, M.; Peters, B.; Huang, W.; Sadow, A. D.; Perras, F. A. Catalytic upcycling of high-density polyethylene via a processive mechanism. *Nat. Catal.* **2020**, *3*, 893−901.
(18) Venkatesh, K. R.; Hu, J.; Wang, W.; Holder, G. D.; Tierney, J. W.; Wender, I. Hydrocracking and Hydroisomerization of Long-Chain Alkanes and Polyolefins over Metal-Promoted Anion-Modified Zirconium Oxides. *Energy Fuels* **1996**, *10*, 1163−1170.
(19) Vance, B. C.; Kots, P. A.; Wang, C.; Hinton, Z. R.; Quinn, C. M.; Thomas H Epps, I.; Korley, L. T. J.; Vlachos, D. G. Single pot catalyst strategy to branched products via adhesive isomerization and hydrocracking of polyethylene over platinum tungstated zirconia. *Appl. Catal., B* **2021**, *299*, No. 120483.
(20) Liu, S.; Kots, P. A.; Vance, B. C.; Danielson, A.; Vlachos, D. G. Plastic waste to fuels by hydrocracking at mild conditions. *Sci. Adv.* **2021**, *7*, No. eabf8283.
(21) Rorrer, J. E.; Beckham, G. T.; Román-Leshkov, Y. Conversion of polyolefin waste to liquid alkanes with Ru-based catalysts under mild conditions. *JACS Au* **2021**, *1*, 8−12.
(22) Rorrer, J. E.; Clara, T.-V.; Beckham, G. T.; Román-Leshkov, Y. Hydrogenolysis of polypropylene and mixed polyolefin plastic waste over Ru/C to produce liquid alkanes. *ACS Sustainable Chem. Eng.* **2021**, *9*, 11661−11666.
(23) Kots, P. A.; Liu, S.; Vance, B. C.; Wang, C.; Sheehan, J. D.; Vlachos, D. G. Polypropylene plastic waste conversion to lubricants over Ru/TiO2 catalysts. *ACS Catal.* **2021**, *11*, 8104−8115.
(24) Lee, W.-T.; Bobbink, F. D.; van Muyden, A. P.; Lin, K.-H.; Corminboeuf, C.; Zamani, R. R.; Dyson, P. J. Catalytic hydrocracking of synthetic polymers into grid-compatible gas streams. *Cell Rep. Phys. Sci.* **2021**, *2*, No. 100332.
(25) Chen, L.; Meyer, L. C.; Kovarik, L.; Meira, D.; Pereira-Hernandez, X. I.; Shi, H.; Khivantsev, K.; Gutiérrez, O. Y.; Szanyi, J. Disordered, sub-nanometer Ru structures on CeO2 are highly efficient and selective catalysts in polymer upcycling by hydrogenolysis. *ACS Catal.* **2022**, *12*, 4618−4627.
(26) Chen, L.; Zhu, Y.; Meyer, L. C.; Hale, L. V.; Le, T. T.; Karkamkar, A.; Lercher, J. A.; Gutiérrez, O. Y.; Szanyi, J. Effect of reaction conditions on the hydrogenolysis of polypropylene and polyethylene into gas and liquid alkanes. *React. Chem. Eng.* **2022**, *7*, 844−854.
(27) Jia, C.; Xie, S.; Zhang, W.; Intan, N. N.; Sampath, J.; Pfaendtner, J.; Lin, H. Deconstruction of high-density polyethylene into liquid hydrocarbon fuels and lubricants by hydrogenolysis over Ru catalyst. *Chem Catal.* **2021**, *1*, No. 437.
(28) Jing, Y.; Wang, Y.; Furukawa, S.; Xia, J.; Sun, C.; Hulsey, M. J.; Wang, H.; Guo, Y.; Liu, X.; Yan, N. Towards the circular economy: converting aromatic plastic waste back to arenes over Ru/Nb2O5 catalyst. *Angew. Chem., Int. Ed.* **2021**, *60*, 5527−5535.
(29) Abbasi, T.; Abbasi, S. A. 'Renewable' hydrogen: Prospects and challenges. *Renewable Sustainable Energy Rev.* **2011**, *15*, 3034−3040.
(30) Dawood, F.; Anda, M.; Shafiullah, G. M. Hydrogen production for energy: An overview. *Int. J. Hydrogen Energy* **2020**, *45*, 3847−3869.
(31) Weitkamp, J. Catalytic hydrocracking-mechanisms and versatility of the process. *ChemCatChem* **2012**, *4*, 292−306.
(32) Database of Zeolite Structures, 2022. http://www.iza-structure.org/.
(33) Kresnawahjuesa, O.; Gorte, R. J.; Oliveira, D. D.; Lau, L. Y. A simple, inexpensive, and reliable method for measuring Bronsted acid site densities in solid acids. *Catal. Lett.* **2002**, *82*, 155−160.
(34) Katada, N.; Suzuki, K.; Noda, T.; Sastre, G.; Niwa, M. Correlation between bronsted acid strength and local structure in zeolites. *J. Phys. Chem. C* **2009**, *113*, 19208−19217.
(35) Chorkendorff, I.; Niemantsverdriet, H.*Concepts of Modern Catalysis and Kinetics*, 3rd ed.; Wiley-VCH, 2017; pp 203−204.
(36) Zichittella, G.; Ebrahim, A. M.; Zhu, J.; Brenner, A. E.; Drake, G.; Beckham, G. T.; Bare, S. R.; Rorrer, J. E.; Román-Leshkov, Y. Hydrogenolysis of Polyethylene and Polypropylene into Propane over Cobalt-Based Catalysts. *JACS Au* **2022**, No. 402.
(37) Bond, G. C.; Yahya, R.; Coq, B. Hydrogenolysis of Alkanes Part 5.- Effect of Metal Dispersion in Ruthenium/Alumina Catalysts on the Hydrogenolysis of Propane and of n-Butane. *J. Chem. Soc., Faraday Trans.* **1990**, *86*, 2297−2301.
(38) Coq, B.; Bittar, A.; Figueras, F. Hydrogenolysis and Isomerization of Alkanes on Ru/Al2O3, Catalysis of Varying Dispersions. *Appl. Catal.* **1990**, *59*, 103−121.
(39) Lewis, J. D.; Ha, M.; Luo, H.; Faucher, A.; Michaelis, V. K.; Román-Leshkov, Y. Distinguishing active site identity in Sn-Beta zeolites using 31P MAS NMR of adsorbed trimethylphosphine oxide. *ACS Catal.* **2018**, *8*, 3076−3086.
(40) Zhou, Y.; Mu, Y.; Hsieh, M. F.; Kabius, B.; Pacheco, C.; Bator, C.; Rioux, R. M.; Rimer, J. D. Enhanced surface activity of MWW zeolite nanosheets prepared via a one-step synthesis. *J. Am. Chem. Soc.* **2020**, *142*, 8211−8222.

https://doi.org/10.1021/acscatal.2c03596
ACS Catal. 2022, 12, 13969−13979